Crystalline Nanojoining Silver Nanowire Percolated Networks on Flexible Substrate

Qiong Nian,[†,‡] Mojib Saei,[†,‡] Yang Xu,[‡,∥] Ganguli Sabyasachi,[⊥] Biwei Deng,[†,‡] Yong P. Chen,[‡,∥] and Gary J. Cheng[*,†,‡,§]

[†]School of Industrial Engineering, Purdue University,315 North Grant Street, West Lafayette, Indiana 47907, United States, [‡]Birck Nanotechnology Center, Purdue University,1205 West State Street, West Lafayette, Indiana 47907, United States, [§]Department of Mechanical Engineering, Purdue University, 585 Purdue Mall, West Lafayette, Indiana 47907, United States, [∥]Department of Physics and Astronomy, Purdue University, 525 Northwestern Avenue, West Lafayette, Indiana 47907, United States, and [⊥]Air Force Research Laboratory, 2941 Hobson Way, Dayton, Ohio 45433, United States

ABSTRACT Optoelectronic performance of metal nanowire networks are dominated by junction microstructure and network configuration. Although metal nanowire printings, such as silver nanowires (AgNWs) or AgNWs/semiconductor oxide bilayer, have great potential to replace traditional ITO, efficient and selective nanoscale integration of nanowires is still challenging owing to high cross nanowire junction resistance. Herein, pulsed laser irradiation under controlled conditions is used to generate local crystalline nanojoining of AgNWs without affecting other regions of the network, resulting in significantly improved optoelectronic performance. The method, laser-induced plasmonic welding (LPW), can be applied to roll-to-roll printed AgNWs percolating networks on PET substrate. First principle simulations and experimental characterizations reveal the mechanism of crystalline nanojoining originated from thermal activated isolated metal atom flow over nanowire junctions. Molecular dynamic simulation results show an angle-dependent recrystallization process during LPW. The excellent optoelectronic performance of AgNW/PET has achieved $R_s \sim 5\ \Omega$/sq at high transparency (91% @$\lambda = 550$ nm).

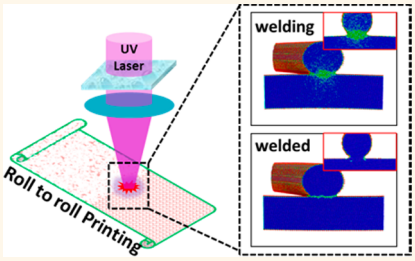

KEYWORDS: silver nanowire · laser plasmonic welding · junction · roll to roll printing · percolation

Owing to their wide application in today's ubiquitous flat panel displays and touch screen technologies, as well as thin-film solar cells and light emitting diodes, transparent and conductive electrodes (TCEs) have drawn increasing attention.[1] Various types of TCEs have been developed for these optoelectronics devices, such as indium doped tin oxide (ITO) and aluminum doped zinc oxide (AZO) which are the standard compounds for most applications performing outstanding optoelectronic property.[2] However, these oxides required high vacuum deposition, which is accompanied by issues like instrumental complexity, high cost and limit scalability.[3] This brittle metal oxide film also does not fulfill the demand of cutting edge flexible electronics. Thus, alternatives like single-wall carbon nanotubes (CNTs),[1,4,5] graphenes[6] and silver nanowires (AgNWs)[7] have been intensively investigated for replacement, attributable to low-cost material synthesis, scalable film fabrication and inherent flexibility.

However, AgNWs film fabrication still suffers from the problem of excessive agglomeration which would deteriorate electrical field distribution and visible range transparency, especially when AgNWs have high aspect ratio (such as ~35 nm in diameter and ~15 μm in lengths).[7] Besides, for AgNWs network corresponding to transmittance of 85−95%, conduction is typically dominated by percolation through junctions with relative large nanowire cross junction resistance (MΩ).[8−10] A variety of attempts have been made to decrease the sheet resistance by improving the junction contacts, including self-forming of nanowires,[11] thermal annealing under pressure[12] and electroplating.[7] But none of these are suitable with cutting-edge agglomeration-free roll-to-roll printing techniques, especially printing on low melting point PET substrate. In addition, it also has been

* Address correspondence to gjcheng@purdue.edu.

Received for review June 13, 2015 and accepted September 21, 2015.

Published online September 21, 2015
10.1021/acsnano.5b03601

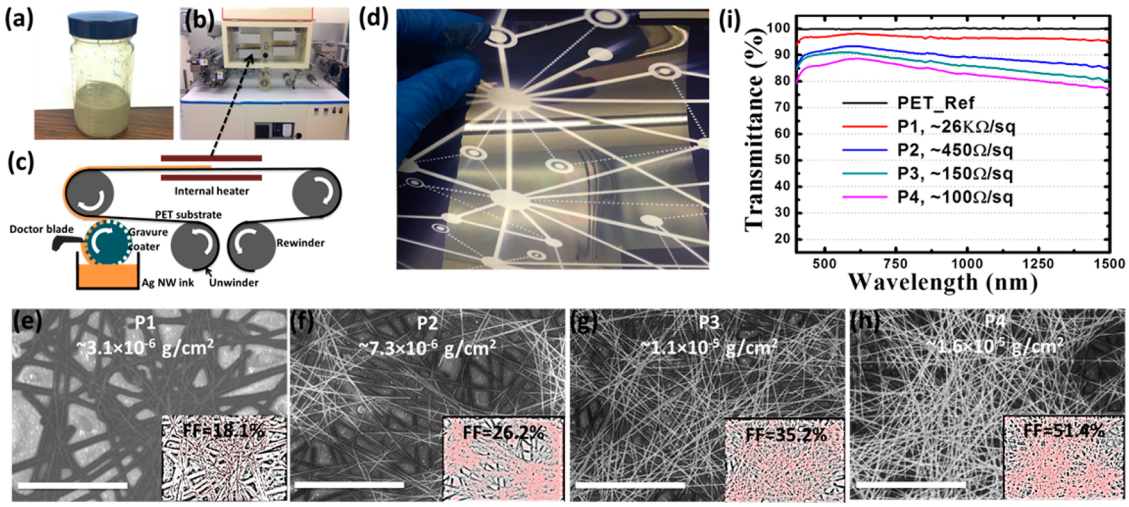

Figure 1. (a) AgNW ink dispersed in ethanol at a concentration of 2.5 mg mL^{-1} used in roll to roll printing; (b) the commercial scale roll-to-roll printing system; (c) schematic setup of the roll-to-roll printing system; (d) an 8 in. × 4 in. uniform printing of AgNWs on a PET substrate. The SEM observation of the printed AgNW film on PET substrate in 4 different area densities: (e) P1 = ~3.1 × 10^{-6} g cm^{-2}; (f) P2 = ~7.3 × 10^{-6} g cm^{-2}; (g) P3 = ~1.1 × 10^{-5} g cm^{-2}; (h) P4 = ~1.6 × 10^{-5} g cm^{-2}. The scale bar is 5 μm. (i) Measured sheet resistance (15% variance) and optical transmittance of printed AgNW film according to 4 different area densities.

challenging to reduce the sheet resistance to below 10 Ω/sq, simultaneously holding the transparency over 90%. While, UV lamp induced optical welding of AgNWs has been invented by Garnett *et al.* recently, which brings a potential for directly improving nanowire junction conductance,[9] during the optical welding, large ohmic losses of metals enable effective light concentration and serve as efficient light driven sources of heat[9] to weld crossed nanowires.

Furthermore, the illustration of rapidly raising and lowering the temperature in nanoscale metallic structures with the use of pulse laser[13−15] suggests that the optical welding, depending on material absorption and the light intensity, can be more effective and efficient if equipped with high speed and high power laser. In addition, laser beam processing time usually ranged from nanoseconds to microseconds, which is favorable for localized fusion of AgNWs without affecting other areas. This direct, efficient and selective laser processing[16,17] could achieve high speed roll-to-roll integration of nanomaterials.

In this work, we investigated the ultrafast laser-induced plasmonic welding (LPW) to assist the commercial scalable roll-to-roll printing of AgNWs on PET substrate. The printing process is based on Meyer rod coating technique to deposit high respect ratio AgNWs (~35 nm in diameter and ~15 μm in length) network on flexible PET substrate as shown in Figure 1c. The printing line speed reaches as high as 1.5 m/min with outstanding film quality. Then, a pulsed laser scans to generate local fusion of AgNW and improve cross junction contacts. The controlled pulsed laser irradiation sparks heat generated at nanowire junctions due to electromagnetic field concentration that occurs in the nanoscale gap between two crossed nanowires.[9,15] As a consequence, thermally activated isolated silver atoms flow over nanowire junction and recrystallize to solder point. The classical percolation calculation is studied to explore the relationship between the macroscale film performance and the microscale nanojunction resistance. And to delve into the mechanism of microscale nanojunctions resistance decrease by LPW, molecular dynamics modeling was carried out to confirm the ultrafast laser-induced nonequilibrium welding, agreeing well with experimental characterizations. These thoroughly understanding of laser-induced plasmonic welding has not been reported before.[15,18] The LPW method improves nanowire cross junction conductance, and removes the organic ligands used during printing as well, which is beneficial for commercial scale fabrication and application. The resulted thin film performance (R_s ~ 5 Ω/sq and 91% T at λ = 550 nm; R_s ~ 13 Ω/sq and 95% T at λ = 550 nm) has not been unveiled before either, subject to laser-induced welding of metallic nanowire network.[15,18]

RESULTS AND DISCUSSION

AgNW ink was bought from Blue Nano, Inc., in which high aspect ratio nanowires (diameters of ~35 nm and lengths of ~15 μm) were dispersed in ethanol at a concentration of 10 mg mL^{-1}. The ink dispersion was observed to be stable at room temperature and ambient atmosphere for 4 months as shown in Figure 1a. To avoid agglomeration and achieve uniform printing, AgNW ink was sonicated for 5−10 s and shaken by hand for 1−2 min. Figure 1b shows the commercial scaled roll-to-roll printing system. To print a film, 50 mL of ink is poured into tray, #30 MG gravure coater is rolled over the ink, and a doctor blade is assembled to remove excess ink, leaving a uniform thin layer of

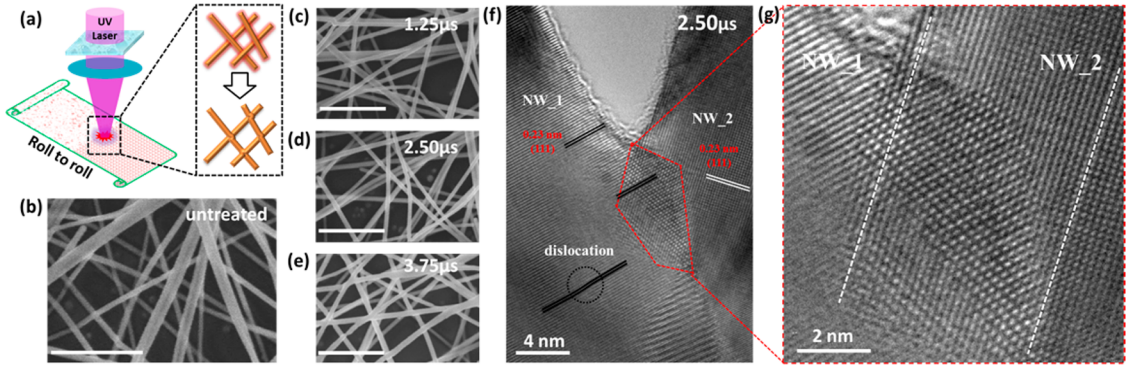

Figure 2. (a) Schematic of the AgNW junction LPW on PET substrate. The nanowires naturally contact with each other, and then enable local heating at junctions by laser exposure. (b) Plane-view SEM images of AgNW film before LPW. Scale bar is 500 nm. Plane view SEM images of AgNW films after LPW with different exposure time: (c) 1.25 μs; (d) 2.50 μs; (e) 3.75 μs. Scale bar is 500 nm. (f) HRTEM image of nanowire junction after 2.50 μs laser exposure. (g) Magnified HRTEM image of joint area formed by LPW.

AgNW ink on the PET substrate with a $\sim$ 60 μm wet thickness. This printing system is a reverse kiss gravure coater, where the coater rotates in the opposite direction to the substrate as shown in scheme of Figure 1c. The kiss coating configuration minimized deflection of the substrate as it passes above the gravure coater, resulting in a small stable bead that combined with the reverse application and finally gives a very good quality and a low coating weight. The liquid thickness is determined by gravure coater rolling speed and wire distribution,[19] that is, the wire diameter and the spacing as mentioned above (#30). Then, the wet coating of AgNW on PET is transferred into internal heater for carefully drying at 110 °C, with translating speed being 1.5 m/min as shown in Figure 1c. The internal heater is applied parallel to PET substrate to avoid uneven local heating, in case of coating agglomeration.[7] Figure 1d illustrates an 8 in. $\times$ 4 in. uniform coating of AgNWs on a PET substrate with a shining star logo underneath.

Figure 1e,f,d,h shows scanning electron microscope (SEM) observation of the printing. It can be seen that uniform, agglomeration-free coating of AgNWs has been achieved. According to our experiment experience and prior reports,[7,19,20] it is found that the ink concentration plays a critical role in tuning the ink viscosity optimally for uniform coatings, which performs best between 1 and 2.5 mg/mL. To boost the efficient manufacturing for commercially scaling up, 2.5 mg/mL concentration is applied. AgNW films with different area densities on PET substrates could be printed, by manipulating ink concentration, wet thickness and coating area. By tuning the density higher, denoted P1 to P4, there are fewer and smaller holes in the films which contribute to better electrical field distribution and conductive performance when used in optoelectronics. The area density increase is estimated by ImageJ calculated surface filling fraction ratio (FF) as well, as shown in insets where FF increases from 18.1% to 51.4%. As the film density decreases from P4 to P1, sparser films with more holes are obtained, which bring negative effect on electrical conduction but perform better optical transparency.[21] Illustrated in Figure 1i, optical transmittance over a large wavelength range is measured with a Vis-IR spectrometer using a blank PET substrate as the reference. P1 with lowest area density of $\sim$3.1 $\times$ 10^{-6} g cm^{-2} (close to classical percolation limit) exhibits highest transmittance over 95% in the full range. As denser films printed, conductance increases from $\sim$26 kΩ/sq to $\sim$45, $\sim$ 150, and $\sim$100 Ω/sq for P1, P2, P3 and P4 with a 15% variation, respectively. However, transmittance decreases to around 80% near-infrared range due to AgNW scattering and reflectance. It is worth to note that visible range transmittances of these 4 different area densities all located over 85% fulfilling requirements of plenty of applications like screen displays, smart windows, and photovoltaics, as well as light emitting diodes.[9]

Right after printing, LPW was carried out on AgNW/PET substrate, with laser parameters mentioned in Experimental Section. Figure 2a shows a schematic of the experimental setup and illustrates the NW−NW junction welding. KrF Excimer laser (λ of 248 nm and τ of 25 ns) beam shaped to a square, top-hat profile (8 $\times$ 8 mm) scans on AgNW films with enabled translations along both *X* and *Y* axis. The laser beam size is adjustable depending on requirement. Nanowire junctions are formed at exposure time of 0.25−3.75 μs for each spot, in laser beam intensity of 20 mJ cm^{-2}. The laser intensity is chosen for nearly negligible heating effect on PET substrate, demonstrated by unchanged PET transparency and XRD signal (Figure 8). The LPW effect was characterized by means of plane-view scanning electron microscopy (SEM), transmission electron microscopy (TEM), optical transmittance and electrical conductivity measurements. Figure 2b−e shows plane view SEM images collected before welding and after different exposure times. Before welding, individual nanowires all over the image were clearly distinct throughout the junctions (Figure 2b). However, the

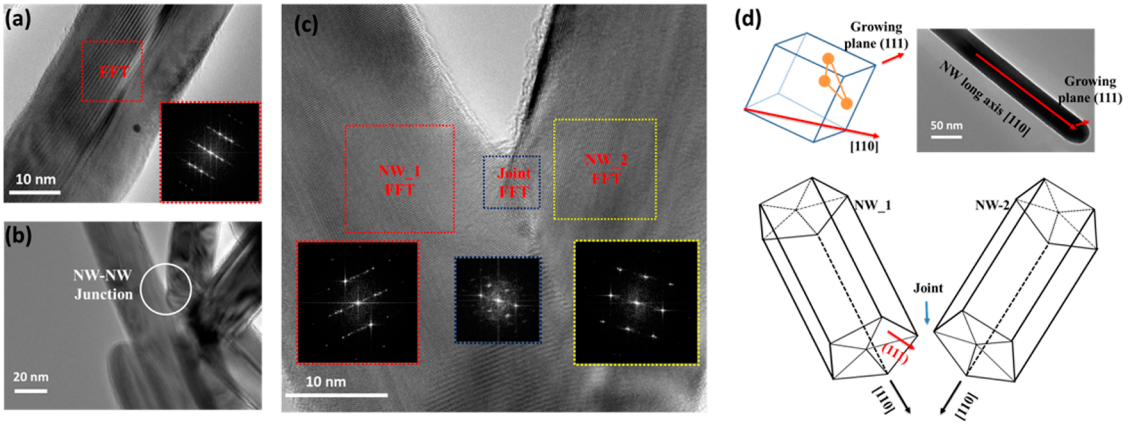

Figure 3. (a) HRTEM image of a single nanowire, while the inset represents the SAED patterns of the nanowire. (b) Low-magnification TEM image of a nanowire junction after LPW. (c) HRTEM of welded junctions; the square represents the size and location of the optical diffraction aperture used for the FFT patterns. (d) Scheme of growing silver nanowire crystal structure, where central axis of nanowire is [111] direction and growing plane is along (111) facets. Nanowires welded together merge over growing plane.

NW−NW junctions subject to 1.25 and 2.50 μs laser exposure get started welding, which is indicated by contrast change at the forming solder point (Figure 2b,c). Apparently, the NW−NW junctions subject to 3.75 μs exposure are welded together completely, which is demonstrated by the solder point formed (Figure 2e). No more exposure time is applied to AgNW films suggested by the electrical measurements.

Further evidence for solder point formation is also provided by high resolution TEM images in Figure 2f,g. As marked by NW_1 and NW_2, two nanowires are slanting downward and merging together. The lattice orientation runs perpendicular cross its length, and lattice fringe measured of 0.23 nm spacing, faying with Ag (111).[22−24] Distinct crystal orientations could be established for two merging nanowires following lattice fringe, represented by the black and white parallel line pairs[22] in Figure 2f. Figure 2g show magnified view of the rhombic area, in which two white lines mark the wire orientation of NW_2. Since the orientation of NW_2 slants bottom left corner, the silver atoms inside the rhombic should originally follow the lattice fringe of NW_2. However, going through NW−NW contact after LPW, it clearly shows lattice orientation of NW_2 was interrupted along the edge of a rhombic area. Inside the rhombic area, atom positions seem following established lattice fringe of NW_1, and simultaneously contributed by NW_2. This reveals a silver atoms recrystallization process during LPW, suggesting laser activated silver atoms around nanojunctions must have exhibited high mobility during ultrafast LPW and allowed the recrystallization onto crystal phase at the solder point area,[9,25] since it is well recognized that the diffusion barrier for a single metal atom surface is quite low (less than 1 eV), which could be easily thermal activated, even at room temperature rather than LPW.[25] However, to create such isolated metal atoms demands a pretty high energy cost, especially with organic ligands coating between nanowires. The ultrafast laser heating is enough to remove organic ligands between nanowires and enable thermal activation, so isolated metal atoms can be created and thus diffused rapidly by means of surface diffusion. On the other hand, lattice fringe at solder point still could be distinguished apparently from NW_1, implying a possible nonequilibrium recrystallization[26] rather than a epitaxial recrystallization;[9] more details are found in Figure SF1. This is owing to ultrashort laser exposure serving as driven force in LPW process (25 ns per pulse). Dislocations could be found in NW_1 according to missing atoms and dislocating atom positions as shown, which ascribe to the nanowire synthesis.

The selected area Fast Fourier Transform (FFT) patterns collected also verified the formation and recrystallization of solder point between contacted AgNWs after LPW, shown in Figure 3. Figure 3a shows a representative TEM image and FFT patterns (equal to optical diffraction patterns) of single nanowire, faying with prior reports, exhibiting pentagonally twined structure sitting on the substrate with one of the five equivalent crystal facets lying flat.[22] The different contrasts inside the twinning boundaries represent the presence of microtwins and stacking faults in silver matrix. These pentagonal twined crystals aroused relatively weak double diffraction spots when comparing to stronger primary patterns along one direction, leading to parallel lines of spots.[9] Figure 3b shows the low-magnification TEM image of nanowire junctions after LPW. The appearance of anomalous contrast change in nanowires is due to overlapping nanowires or a high density of stacking faults in addition to twinning boundaries. The twining structure was mainly observed in nanowires, however, rarely in nanojunctions due to recrystallization process of welding; more images shown in Figure SF2. The nanowire junction is

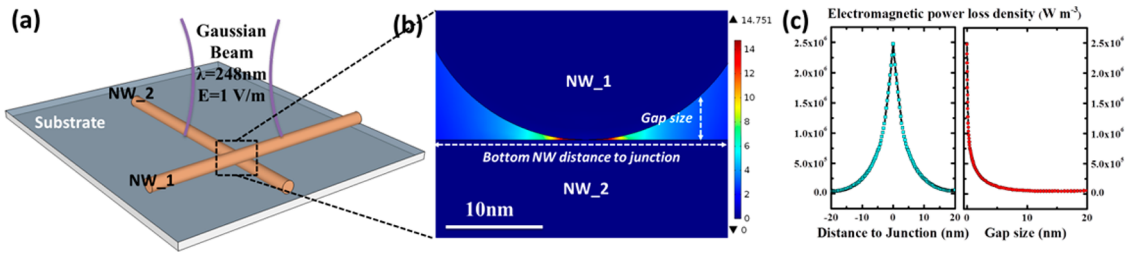

Figure 4. (a) Comsol Multiphysics simulation of LPW on crossed AgNWs: incident laser beam was simulated as a Gaussian electromagnetic wave delivered onto a nanowire cross junction with an electrical field of 1 V/m. AgNWs crossed at 90°, suspended in air and touching each other. Each nanowire was modeled as having a circular cross section with 40 nm diameter and essential physical parameters input. (b) The cross-sectional image of AgNWs on the right-hand side indicates local electrical field distribution, where color legend changes from blue (0 V/m) to red (14 V/m). (c) The heat generation in AgNW as a function of distance to the crossed junction, calculated by power loss density in Comsol Multiphysics, and the heat generation in AgNW junction as a function of gap size between the crossed nanowires.

focus-in viewed and FFT patterns are analyzed in Figure 3c. Comparing NW_1 to NW_2, the diffraction patterns is visible along two different directions, with roughly equal intensity and rotated certain degrees (~45°). Both these two diffraction patterns represent silver nanowires by tilting the silver nanowires around the growth direction of [110] (the long axis of nanowire).[22] However, at the joint after LPW, it is clearly seen that diffraction patterns of solder point correspond to the single crystal with fcc structure along the [110] zone axis direction, indicating recrystallized phase and reorganized atom positions accomplished along the (111) growing plane.[22] The geometry scheme is shown in Figure 3d, in which the fcc lattice of silver nanowire is tilted to be comparable with TEM image taken on right-hand side, showing the two single nanowires were grown along [110] long axis with growing plane of (111). During nanowire LPW process, subcrystals along (111) plane get started to weld together *via* metal atom surface diffusion, in which isolated metal atoms are created by laser heating.[9,22,25,27] The crystal structures of nanowires and the welding process between them provide good agreement with prior statements.[9,22−25,27]

Moreover, it is important to point out that the nanowires away from the junction were unaffected by the laser exposure and no morphology change was observed. However, if higher laser intensity or more exposure time was applied, Rayleigh instability might appear resulting from the photo energy absorption and local high temperature generation of PET substrate,[9,28] as revealed by comparison between panels b (before laser) and e (over exposure) of Figure 2 where necking appeared close to the welding point. The Rayleigh unavoidable instability[9,28] in hot plate treatment shows the strength of the ultrafast LPW, which could enhance the electrical connection by sole junction modification without breaking or changing nanowires.

To understand the mechanism of LPW, we performed a Comsol Multiphysics simulation with a Gaussian electromagnetic wave as incident laser on a cross of nanowire junctions. As presented in Figure 4a, Gaussian beam laser was delivered to AgNWs with an electrical field of 1 V/m, where the diameter of AgNW was set as 40 nm. In simulation, AgNWs were considered crossed at 90°, suspended in air and touching each other. Each nanowire was modeled as having a circular cross-section and with essential physical parameters input. After LPW, local electric field distribution in the crossed nanowire junctions was shown in Figure 4b. As calculated, local electrical field was concentrated as high as 14 V/m near junction area due to surface plasmon polarization,[9,29,30] whereas only 4.5 times enhancement subject to adjacent paralleled nanowires was observed (Figure SF3). This angle dependable field enhancement suggests that laser welding favors the crossed NW junctions over paralleled ones, which nearly would not affect welding quality of random AgNW film printed in this study since crossed junctions dominated. Furthermore and noteworthy, sole nanowire contacts are able to concentrate localized electrical field and form "nano heater", while letting the nanowire away from the junctions remain nearly unaffected.

To further explore the heating process generated by the "nano heater", the electromagnetic power loss density as a function of the distance to junctions and gap size between nanowires was plotted in Figure 4c. The power loss density calculated by Comsol Multiphysics was determined from the illumination power density, which multiplies the metal nanostructures' absorption coefficient (imaginary part of the dielectric function, constant for mono wavelength laser)[31] that indicates the heat generation. Figure 4c illustrates the heat generation limits near AgNW junction (±5 nm) and decreases as distance to junctions increase for bottom nanowire. It implies that the effective zone of LPW is constrained near junctions with about 5 nm variations, providing efficient junction welding without nanowire itself affecting. This is in good agreement with Figure 2 that the nanowire away from junctions remains nearly unchanged. Figure 4c also illustrates that as the gap size between nanowires decreases, the power loss density increases, indicating the heat

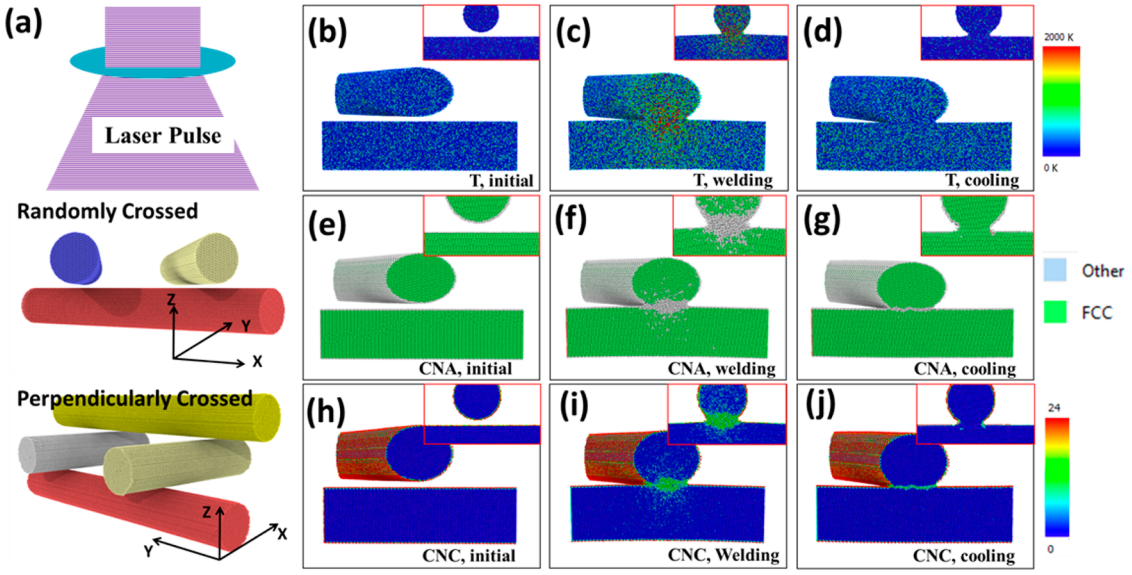

Figure 5. (a) Molecular Dynamic simulation setup of LPW. Laser pulses as incident beam on random angle crossed nanowires and perpendicularly crossed nanowires. Plasmonic heating set as an exponential function of distance to junctions. (b–d) Temperature evolution was represented in cross section view (*XZ* plane slice) in the middle of crossed nanowire junctions (b) initial status, (c) welding status, and (d) cooling status. (e–g)Nanowire fcc crystal structure evolution cross section view (*XZ* plane slice) in the middle of junctions (e) initial status, (f) welding status, and (g) cooling status. (h–j) Nanowire ordering structure evolution cross section view (*XZ* plane slice) in the middle of junctions (h) initial status, (i) welding status, and (j) cooling status. The insets show corresponding status of perpendicularly crossed nanowire junctions.

generation spikes. The apparent heat generation was observed in small gaps like size lower than 5 nm, but still supplying sufficient nanowelding for nanowire junctions usually with a gap size in 2 nm due to organic ligands. As the gap size increases, the power loss density decreases and the heating become less effective, which protects nanowire itself from being overheated.[9,15]

With constrained heat generation around nanowire junctions, to further delve into the joining process and forming structure of solder point, molecular dynamics (MD) simulation was implemented. LAMMPS[32] package was used in this simulation setup. As shown in Figure 5a, silver nanowires either crossed in random angles or perpendicularly were considered in a box with periodical boundaries in all directions. First, NPT ensemble with pressure of 1 atm and equilibrium temperature of 300 K for 100 ps was applied. Then, in NVE ensemble laser heating was considered as a heat source focused in nanowire junctions. To fit with COMSOL simulation, heating was introduced as an exponential function of distance. The maximum in exponential heating is equivalent to 5.6 μeV/fs per atom. Laser heating has been continued for 150 ps and then the heating source was turned off while simulation continued for an additional 500 ps in a NVT ensemble. For this last simulation step, the Nose-Hoover thermostat has been weakened using a time constant equal to 1000 time steps. This is to match simulation with the real case where the structure cools down in air at a slower pace compared to laser heating phase.

In this simulation, the interactions between silver atoms have been simulated using EAM[33] potential extracted from prior work of Williams *et al.*[34] A time step of 1 fs was used during the whole simulation, with OVITO[35] being utilized for visualization. Panels b, c, and d l Figure 5 show temperature evolution of structure after NPT run (initial state), just after laser heating (welding state), and at the end of simulation (cooling state), respectively. These figures show an *XZ* plane cross-sectional view in the middle of junction area. From Figure 5c, it is clear that heat generation was mainly focused near nanowire junctions, though heat diffusion and dissipation occurs, resulting in thermally activated silver atoms created in the junction. The insets show perpendicular nanowire junctions, where silver atoms were activated similarly. Figure 5e–g represent the result of common neighbor analysis (CNA)[36] for equivalent states corresponding to Figure 5b–d, in which perfect fcc structure was marked green, while other disordering structures were marked gray. It is interesting to observe how the structure evolved from the initial structure to a distorted state during welding; however, by going to cooling state, it gradually returns to ordered crystalline structure with apparent grain boundary. The disordering structure formed during welding, attributed to thermally excited atoms tending to vibrate and resist staying in original lattice position. These excited isolated metal atoms possess high mobility, diffusing over nanowire junctions and enabling welding process,[37] while during cooling process, these activated atoms tend to follow

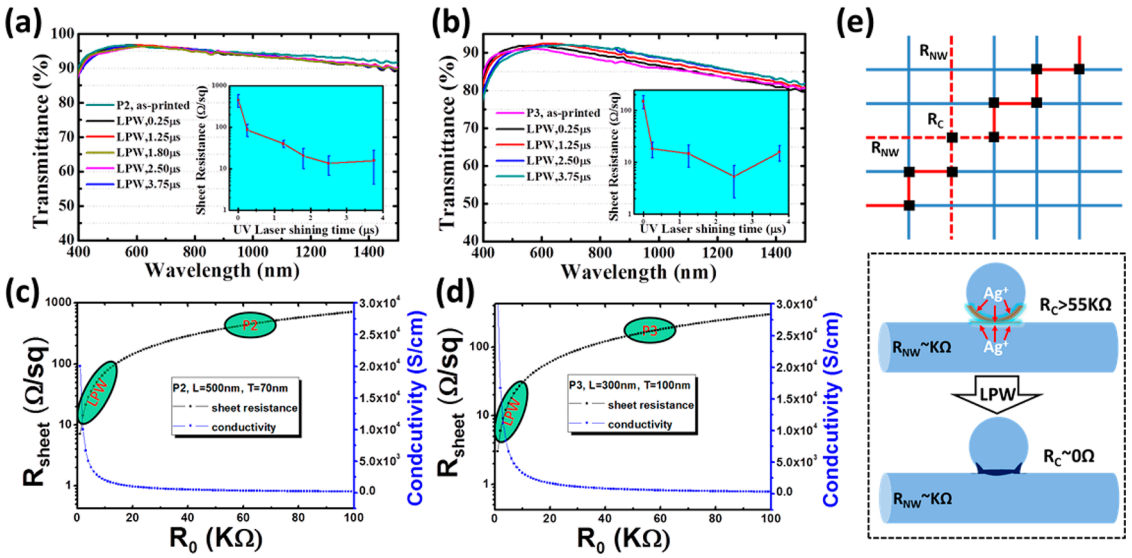

Figure 6. (a) Optical transmittance of P2 AgNW transparent electrode film *versus* wavelength and laser exposure time. The plots show the total diffusive transmittance as a function of wavelength for different exposure time for P2 sample. Inset: P2 AgNW transparent electrode sheet resistance corresponding to laser exposure time. (b) Optical transmittance of P3 AgNW transparent electrode film *versus* wavelength and laser exposure time. Inset: P3 AgNW transparent electrode sheet resistance corresponding to laser exposure time. (c) P2 AgNW film sheet resistance and conductivity as a function of percolation junction resistance R_0, calculated by percolation theory with thickness T of 70 nm and percolated "stick" length L of 500 nm. (d) P3 AgNW film sheet resistance and conductivity as a function of percolation junction resistance R_0, calculated by percolation theory with thickness T of 100 nm and percolated "stick" length L of 300 nm. (e) Scheme of AgNW network conductance dominated by contact resistance through percolating nanowires and the scheme of LPW effect on nanowire contact resistance.

the arrangement of matrix to gain the perfect fcc crystalline structure back due to Binks potential, though 2 layers of atoms formed boundary between different grain orientations. This reflects that although heated junction was distorted, the perfect crystalline structure would be formed due to enough spacing time between laser pulses. This agrees well with TEM observation over nanowire junction in Figure 3, as well as Figure 5h–j, structure disordering degree in lattice structure indicated by Centro-Symmetry parameter[38] (CNC) analysis. As shown, the CNC analysis was done on LPW welded randomly crossed silver nanowires. The color legend on the right-hand side illustrates that the disordering increases when color changes from blue to red. Comparing the three processes shown in the figures, it is clearly seen that during welding process, the silver atoms in both two nanowires were thermally excited tending to vibrate and resist stay in original position. However, in the cooling process, the energy of metal atoms decreases, driving the atoms to reorganize to low energy structure, which is crystallized and ordering structure. A boundary with 2 or 3 layers of atoms was formed due to unmatched lattice orientation between the bottom and top nanowire.

However, upon perpendicular nanowire junction shown in insers of Figure 5e–g, due to perfectly matched lattice orientation of two crossed nanowires, metal atoms inside welding point recrystallize and reorder into single crystal phase (fcc) without any boundaries formed. CNC analysis on the insets of Figure 5h–j verifies this statement as well. Additionally, Figure SF4 also shows the *XZ* plane cross-sectional view of LPW on nanowires crossed in 90° and the corresponding structure in a diagonal slice in *YZ* plane. Thus, an angle-dependable recrystallization process during LPW was demonstrated, providing a guild for further research and application of aligned AgNW device. Movie SM1 also shows the complete evolution of Centro-Symmetry parameter in whole process to further support our statement of ultrafast welding and reordering after cooling state. Movie SM2 represents the flow of atoms and demonstrates how silver atoms from two nanowires mingle to form a uniform junction. The crystalline structure accomplished after LPW would be beneficial for electrical conduction cross nanowire junction, which would be able to enhance macro-scale optoelectronic performance.

To demonstrate the practicality of LPW process in macro-scale applications, we printed large area AgNWs (Figure 1d, 8 in. × 4 in.) on PET for optoelectronic performance evaluation. Because of application in flat panel displays and touch screen technologies, as well as thin-film photovoltaics, high visible transparency and low sheet resistance are required simultaneously. Thus, AgNW films subject to area density of P2 and P3 were printed and welded to achieve best optoelectronic performance. Figure 6a,b monitors visible-IR transmittance (average of large area test) with a bare PET substrate as reference, and 4-point-sheet resistance as a function of laser exposure time. Compared with

as-printed P2 sample in Figure 6a, the wavelength-dependent transmittance remains almost unchanged after LPW, with a slight increase owing to organic ligands removal or minor variations in the nanowire density. Transmittance of 95−96% at 550 nm and over 90% at visible range was obtained for P2 samples subject to both untreated and welded conditions. Then, the inserted figure shows low sheet resistance simultaneously accomplished after LPW, which decreases from 450 to 13 Ω/sq as laser exposure time increases from 0 to 2.50 μs. The sheet resistance drops by a factor of over 30 after 2.50 μs shining, but slightly increases subject to 3.75 μs shining (∼15 Ω/sq). This large drop in resistance is attributed to UV laser nanowelding of nanowire junction, which is usually 3 orders of magnitude higher than single nanowire resistance.[7,9,15,39] However, after laser welding, the dominant individual junction resistance decreases to be comparable with nanowires themselves, leading to incredible low sheet resistance as 13 Ω/sq. This also can be demonstrated by AgNW network sheet resistance calculation according to Kirchoff's rules,[40] where 10−50 Ω/sq would be contributed by solely nanowires themselves. The incredible high transmittance (95% *T* at 550 nm) and simultaneously low sheet resistance (13 Ω/sq) have not been reported before, which is comparable to bulk silver grid fabricated with perfect bulk junction between crossed grids. However, the transmittance of current sample (95% *T* at 550 nm) performs much higher than bulk silver grid, implying the superiority of LPW processed AgNW network. The slight increases subject to overexposure of 3.75 μs resulted from the randomly formed necking area in specific nanowires as mentioned above, since the stretched morphology along rod axis during necking would increase the resistance of nanowire itself. Thereby optimal laser exposure time play a crucial role. To further enhance electrical conductance, P3 sample subject to higher nanowire area density was investigated as shown in Figure 6b. The lowest sheet resistance of 5 Ω/sq was achieved by 2.50 μs UV laser exposure as well. However, the slight increase to 15Ω/sq after 3.75 μs UV laser shining implies the Rayleigh instability[9,28] might be introduced by excessive heat generation from nanowire surface Plasmon or PET substrate absorption. The visible-IR transmittance of P3 sample is also nearly unaffected before and after LPW, encountering slight variations similar to P2. Relative lower transmittance of 91−92% at 550 nm and over 85% at visible range was obtained owing to higher nanowire area density. The best optoelectronic performance of 5 Ω/sq and simultaneous 91% *T* at 550 nm was also remarkable to the author's knowledge. It reveals that the LPW has the potential to implant into commercial scale fabrication like roll-to-roll printing to fulfill the demand of enhancing AgNW TCE optoelectronic performance during printing.

Classical percolation theory was referred to further calculate the nanowire junction resistance and the film sheet resistance, in order to clarify the electrical conductance improvement by LPW. As shown in eq 1, Stauffer *et al.*[10,12,41] state that, "sticks" (nanotubes and nanowires) randomly distributed throughout an insulating medium adhere to the following relation:

$$\sigma \propto (N - N_c)^t \tag{1}$$

where σ is film conductivity, N_c is the minimum wire density (per area for a 2-D film; per volume for a 3-D film) required to achieve conductivity from one side to the other, N is the actual wire density within the film, and t is the critical exponent which accounts for dimension and percolation model. Then, Foygel *et al.*[10] advance the equation to calculate the "sticks" percolated film conductivity, considering wire density and aspect ratio as shown in eq 2.

$$\sigma \cong \left[R_0 l \left(\frac{0.6}{\alpha} \right)^t \right]^{-1} \tag{2}$$

where R_0 is the resistance of the nanowire or of the contact between nanowires, whichever is larger. l is the typical distance between the contacts, which decreases as nanowire area density increases due to crisscross. a is the aspect ratio of the nanowire and $t = 1.4$ for our AgNWs network.[10] To calculate film sheet resistance, eq 3 is drawn to divide film resistivity by thickness, where T indicates estimated film thickness.

$$R_{sheet} \cong \left[R_0 l \left(\frac{0.6}{\alpha} \right)^t \right] / T \tag{3}$$

Figure 6c,d plots the film conductivity and sheet resistance as a function of R_0, according to eqs 2 and 3, in which $l \sim 500$ nm and $T \sim 70$ nm for P2 and $l \sim 300$ nm and $T \sim 100$ nm for P3 are assumed by pane view SEM images and ImageJ software calculation. Apparently, after laser welding, to obtain ∼13 Ω/sq for P2, R_0 should be <2 kΩ, revealing that the contact resistance between nanowire junctions becomes comparable or negligible to that of nanowires themselves (R_{NW}). Directly calculated R_{NW} could be as low as ∼0.25 kΩ for a single AgNW with 15 μm in length and 35 nm in diameter, whereas actually value usually approaches one or several kilo-ohms[9] probably because of oxidation degrading and organic ligands coating. Therefore, after LPW, taking off R_{NW} contribution to R_0, the contact resistance cross nanowires could be estimated as 0 Ω. However, before welding, R_{sheet} subject to P2 is ∼450Ω/sq, and this corresponds to R_0 of >60 kΩ revealing that junction resistance is dominant. As well as P3, R_0 is decreased from >55 to <2 kΩ after laser welding as well, according to sheet resistance change. This change implies the dominant resistance of NW−NW junctions has been decreased by

(a)

Junction	R_{NW} (NW1)	R_{NW} (NW2)	R (Cross junction)
J1 (before)	280Ω	625Ω	Almost Open (>MΩ)
J2 (before)	365Ω	328Ω	Almost Open (>MΩ)
J1 (after)	280Ω	625Ω	490Ω
J2 (after)	365Ω	328Ω	360Ω

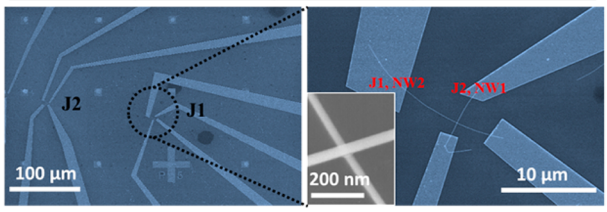

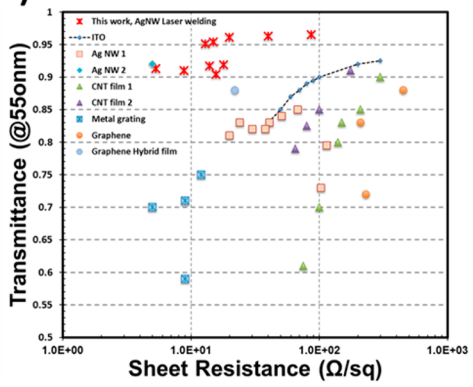

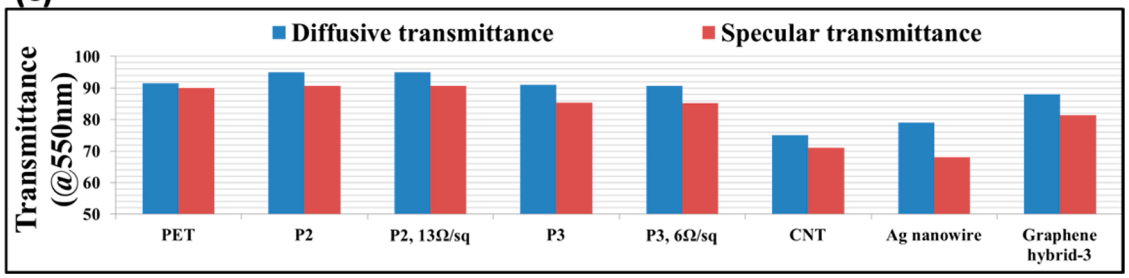

Figure 7. (a) Individual silver nanowire and junction resistance. The table shows 2 point test for single silver nanowires and crossed nanowire junctions before and after 2.50 μs exposure. The welded junction shows a comparable resistance to the single nanowire itself, indicating excellent electrical contact. The inset shows SEM images of welded junctions with scale bar of 200 nm. (b) Optical transmittance at 550 nm wavelength of laser welded P2 and P3 AgNW TCE as a function of sheet resistance. The performance of ITO, CNT, graphene, and metal gratings are shown for comparison. (c) Diffusive and specular transmittance of PET substrate; CNT on glass according to ref 7; Ag nanowire on glass according to ref 7; graphene hybrid on glass according to ref 42; and P2, P3 AgNW on PET substrate. The differences in the diffusive and specular transmittance indicate the scattering of the light by the material.

LPW, and finally becoming comparable or negligible to single nanowire resistance, as illustrated in Figure 6e.

This electrical conductance improvement of nanowire and corresponding junction after LPW could be further confirmed by monitoring four point tests of spray-coated and Laser plasmonic welded AgNWs on top of silicon dioxide/silicon substrate, where the contact resistance between nanowires (R_C) was expected to be critical. Couple of nanowire pairs and junctions was fabricated (E-beam lithography) and measured before/after LPW, only two were shown in Figure 7a. Nicole/gold metallization was utilized as electrodes to connect nanowire with macro-scale testing probes (Figure 7a, J1 and J2). Comparing J1 and J2 (before LPW) junctions to after LPW junctions, we found that the electrical conductance of nanowire itself was stable, ranging from 280 to 625 Ω depending on target wire length. The nanowire conductance is consistent with our calculations and previous statements. On the other hand, cross junction resistance between nanowires, from ~MΩ (approaching voltmeter limit), drops significantly after LPW to be comparable with nanowire itself as tested in Figure 7a. Taking off half nanowire resistance from the cross junction resistance, it reveals contact resistance between nanowires approaching ~0 Ω. This drop from near open to ~0 Ω indicates macro-scale percolating film performance is dominated by nanowire contact resistance before LPW, but after LPW also has major contributions from nanowire itself because of comparable R_{NW} and R_C, which are achieved in percolation theory. In addition, there are a few junctions possessing better electrical path before LPW in our experiments, rather than ~MΩ cross junction resistance, which probably averages R_0 to 55−60 kΩ in percolation theory calculation discussed above.

In sum of the optoelectronic performance evaluation, the transmittance at 550 nm of current series of direct laser welded AgNW films was plotted as a function of film sheet resistance in Figure 7b and compared to experimental data for ITO thin films[42] and other developed transparent electrode alternatives such as metal gratings,[43] CNT random meshes,[4,5,44] referring AgNWs[7,37] and graphene/hybrid graphene.[6,45] All of these transparent electrodes need to compromise the transmittance to achieve lower sheet resistance (<100 Ω/sq), with which AgNW films perform similarly. However, the uniformly printed films with high aspect ratio Ag nanowires could accomplish ~13 Ω/sq and 95% transmittance (P2), which show more competitiveness than ITO thin film in the mainstream market and the cutting age alternatives. AgNW films subject to

higher density (P3) could achieve ~5 Ω/sq and 91% transmittance due to higher reflectance and scattering.[7] This mass-produced AgNW films show superior performance, which simultaneously possessing low cost solution based fabrication, uniform roll-to-roll printing and efficient LPW could immediate commercial scale manufacturing.

On the other hand, the transmittance in current study was measured by lambda 950 with an integrating sphere to integrate all forward light including both specular transmitted and scattered transmitted. The specular transmittance indicates the light comes out of the sample parallel to the incident light. The difference between the diffusive and specular transmittance is generally utilized to evaluate the light scattering which might trigger problematic for flat panel displays and touch screens[7,45] (Figure SF5). To measure the light scattering, the baseline for the spectroscopy is set by scanning a blank PET substrate and then AgNW film is installed on a solid sample holder between light source and the detector. The diffusive and specular transmittance data are obtained at 550 nm wavelength, and the difference between them is shown in Figure 7c comparing with other transparent electrode alternatives.[7,45] It can be seen that the scattering of AgNW film on PET substrate after LPW is ~4.2% and ~5.6% subject to P2 and P3 density, respectively. Considering approximate 2% light scattering contributed by PET itself (1% for glass substrate), only ~2.2% and 3.6% result from P2 and P3 metal nanowire scattering. Taking off the scattered transmitted light, the pure specular transmittance of P2 and P3 samples achieve 92.8% and 87.4%, which are also outstanding performance and fulfill industrial requirements. Relative higher nanowire density will result in larger light scattering, which is consistent with metal nanowire optical property.[7] However, it is lower than prior reports of Ag nanowire (~10%)[7] and AgNW-Graphene hybrid film[45] (h3, ~6.6%), attributing to slimmer nanowires and more uniform printing. As we know, the fabrication of uniform film of AgNW with high aspect ratio of 35 nm in diameter and 15 μm in length remained an issue before this study. Comparing with single walled carbon nanotubes network (~3%), P2 sample is more competitive. But it is additionally desired to note that CNT loses transmittance due to absorption, while AgNW films lose transmittance due to scattering, not absorption.[46] Unfortunately, current series of samples still suffer from competing with traditional transparent conductive oxide (TCO) like ITO (~1%).[7,45] However, due to flexible and stretchable electronic devices demand, nanowire percolated networks would be favorable over brittle TCO, especially for light scattering preferred device like thin film photovoltaics.

To explore the flexibility of welded AgNW film which might be utilized in future flexible optoelectronic devices, mechanical related characterizations were carried out including bending sheet resistance (Figure 8a) and peeling off test (Figure SF6). As shown in Figure 8a, the resistance measurements of AgNW/PET with curvature from 0 to 0.06 mm^{-1} were carried out to test the bending flexibility. It was detected that P2 and P3 samples (before LPW) possess pretty stable conductance during bending, comparing to standard brittle ITO film. However, there are still fluctuations observed due to not welded cross nanowire junction. After LPW, P2 and P3 achieve ultrastable conductance during bending, though negligible fluctuations felling into the scope of conductance deviation, illustrating outstanding flexibility in current series of samples.[45] To test the mechanical stability of the printed AgNW network on PET, a thin layer of polydimethylsiloxane (PDMS) was coated, cued and then peeled off from the top surface. After peeling test, the AgNW network stayed on the surface of PET substrate as shown in Figure SF6, though nanowire ends point upward owing to PDMS adhesion force. This phenomenon also has been reported by Madaria *et al.* in AgNW PDMS dry transfer technique.[12] It reveals high surface energy between thin/long AgNW film and the PET substrate, suggesting acceptable mechanical stability. Finally, chemical stability was tested in ambient atmosphere as shown in Figure SF7. The sheet resistance of P2 and P3 samples under different laser welding conditions was tested after 3 months; comparing with right after roll-to-roll printing combined LPW, the evaluation reveals that electrical conductance nearly maintains unchanged after long period of time. The stable electrical property is important for practical macro-scale application even though protective package will be added in commercial fabrication.

To illustrate that PET substrate has capability to sustain in LPW, bare PET substrates subject to all laser exposure conditions were characterized by Vis-IR transmittance and X-ray diffraction (XRD) patterns in Figure 8b,c. As shown in Figure 8b, extremely slight transmittance change was detected after up to 3.75 μs exposure, comparing with untreated one. This reveals that the laser exposure will not affect the optical performance of current series of samples. Figure 8c plots the XRD patterns of PET substrates, before and after laser exposure, showing unchanged PET structure due to untra-short exposure time, small heat-effective zone and fast processing speed, consistent with prior reports.[47] Both optical performance and structure test further confirm the nearly unaffected substrate during LPW after roll-to-roll printing, which is helpful for large-scale manufacturing. The effects of laser exposure time and laser intensity on macroscale film performance were investigated. As demonstrated in Figure SF9, too high laser intensity would bring overexposure issue of the nanowire network, in which selected area of nanowires are broken, fragmented to short sections

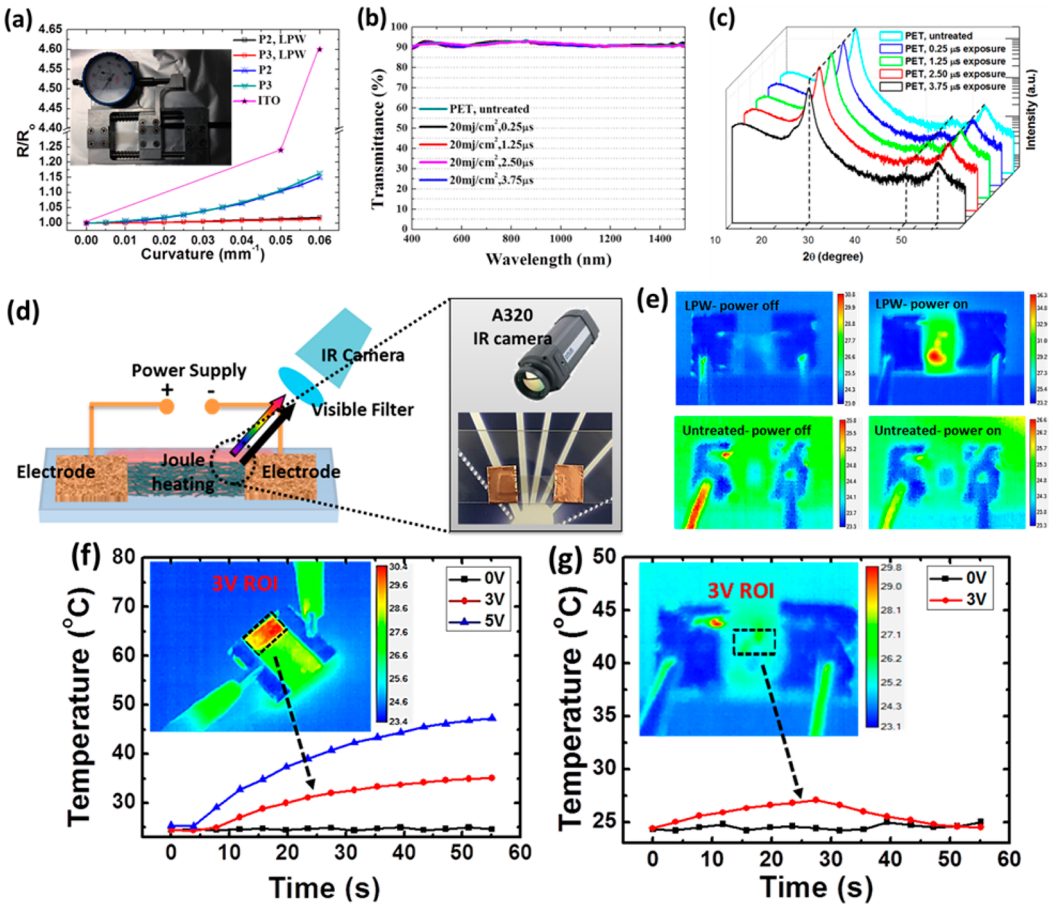

Figure 8. (a) The ratio of bending resistance to original resistance as a function of bending curvature before and after LPW for P2 and P3 samples, comparing to standard ITO film. The inset shows the designed bending gadget. (b) Optical transmittance of bare PET *versus* wavelength and laser exposure time. The plots show the total diffusive transmittance as a function of wavelength for different exposure time for PET substrate. The diffusive transmittance include both specular transmitted and scattered light collected by integrating sphere. (c) XRD patterns of bare PET as a function of laser exposure time. The plots show PET structure change according to different exposure time. (d) The scheme of transparent heater performance measurement. (e) The joule heating comparison between LPW processed AgNW film and the untreated one. (f) The temperature as a function of time during continuous joule heating of LPW processed AgNW film. (g) The temperature as a function of time during continuous joule heating of untreated AgNW film.

and even degraded to nanobeads. Therefore, laser intensity should be carefully optimized in practical application.

The device level application of the AgNWs network as a transparent heater was demonstrated in Figure 8d–f. Figure 8d shows scheme of the fabrication and measurement of transparent heater. The LPW processed AgNW/PET film were tailored to specific size and followed by electrode fabrication onto two ends. A voltage-tunable power supply was utilized to mimic the situation when applied in practical applications like thermal windows or anti-icing devices. An FLIR A320 thermal camera with visible filter was utilized to capture joule heating picture and the temperature evolution. The inserted pictures on the right-hand side are the demonstration of the sample film and the camera. Figure 8e shows the comparison of heating performance between AgNWs films with and without LPW treatment. For the sample subject to LPW processing, the surface temperature could be increased to around 32 °C (on average) with peak temperature achieving 36 °C, when direct power was on (3 V). The corresponding surface temperature before power on stays at around 25 °C. On the other hand, for the AgNWs thin film without LPW, due to nonstabilized nanojunctions with high resistance, the macro scale film is apt to be broken-down; therefore, no temperature increase can be observed, as demonstrated in Figure 8e. Figure 8f revealed that temperature rises rapidly with adjustable electrical voltage applied to the transparent heaters. As shown in the plots of film temperature as a function of time period during direct power supply, comparing to around 25 °C on average for 0 V voltage supply, the average temperature of the ROI (region of interest in the inset) could achieve 35 and 47 °C in 60 s, with 3 and 5 V voltage supply on, respectively. The inserted IR image in Figure 8f shows the sample ROI during 5 V power supply on, in which peak temperature can even reach around 60 °C. The nonuniform surface joule heating due to local heat accumulation or nanowires

area density variation, which might be able to be solved by wrapping thermally conductive 2D materials like graphene, which are under investigation in future works. Figure 8g plots the surface temperature as a function of time period during direct power supply on for untreated AgNWs film, in which the average temperature of the ROI could not achieve beyond 28 °C and even followed by cooling down (electrical breakdown), with 3 V voltage supply on. The much lower temperature responses are results of high electrical resistance between the junctions of the AgNWs without LPW, and potential damage caused by the electrical discharge when two nanowires are very closely touching but not completely connected.

CONCLUSION

In summary, the high speed LPW provides direct, efficient and selective generation of NW−NW crystalline junction in roll-to-roll printed AgNWs percolated networks. The optoelectronic performance is dramatically improved: R_s as low as 5 Ω/sq at high transparency (91% at λ = 550 nm), which indicates cross nanowire junction resistance is comparable to the resistance of nanowire themselves, according to classic percolation theory and four points tests. The physical mechanism of LPW contributes to constrained heat generation at nanowire junctions that tend to create isolated metal atoms, which has high mobility, flow over junction surface and weld nanowires. Angle-dependable recrystallization process during LPW is discovered, providing a guideline for future research and fabrication of aligned AgNW device. These are demonstrated by COMSOL multiphysics simulation and molecular dynamic simulation. The laser beam could be focused, directed, and programmed by beam scanning systems, which enable commercial scale manufacturing of AgNW TCE, such as roll-to-roll printing with capability to print uniform thin and long AgNWs without any agglomeration. The optoelectronic property of welded AgNWs TCE film is superior to typical reported values of ITO and other alternatives. Excellent mechanical and chemical stabilities of the AgNW thin films after LPW are also demonstrated. AgNWs network after LPW has been demonstrated as a good transparent heater. These results provide the guidance of LPW for nanoscale integration of nanomaterials for their applications in screen displays, solar panels, smart windows and other optoelectronic devices.

EXPERIMENTAL SECTION

Printing. Commercial AgNWs (Blue Nano, Inc., NC) with diameters of ~35 nm and lengths of 15−30 μm were dispersed in ethanol at a concentration of 2.5 mg mL^{-1}. AgNWs network were roll-to-roll printed onto flexible PET web, where the parameters of roll-to-roll system including PET web tension, micro roll speed and line speed need to be controlled for better printing quality. The line speed used in current study was 1.5 m min^{-1} for efficient printing. Higher line speed resulted in sparser nanowire area density, and can be densified by higher micro roll speed. Right after printing, the as coated film would be translated to an internal heater for further drying with an automatic scroll system. The whole system is shown in Figure 1b.

Welding. Then KrF excimer laser (λ of 248 nm and τ of 25 ns) with repetition rate (RR) of 10 Hz was directed to the AgNW network to improve the cross-wire junctions. To efficiently process large-scale film, the laser beam was shaped to a square, top-hat profile (8 × 8 mm) and enabled translations along both *X* and *Y*-axes. Laser intensity utilized in the welding is 20 mJ cm^{-2}, and the exposure time of each spot ranged from 0.25 to 3.75 μs corresponding to 10−150 pulses. The laser beam with line shape and higher repetition rate is taken into account to boost process speed even more and immediate efficient commercial scale manufacturing.

Characterization. After welding, field emission scanning electron microscopy (FE-SEM, S4800) was used to observe the plane-view surface morphology. The nanowire density can be

TABLE 1. Nomenclature, Greek Symbols and Abbreviations Used in This Study

	nomenclature
l	typical distance between contacts (nm)
N_C	minimum wire density (cm^{-2})
R_C	Contact resistance (Ω)
R_{NW}	Nanowire resistance (Ω)
R_{sheet}	Sheet resistance (Ω)
t	critical exponent
T	thickness (nm)
X	coordinate
Y	coordinate
Z	coordinate
	Greek symbols
α	aspect ratio of the nanowire
σ	Film conductivity (s m)
λ	wavelength (nm)
	abbreviations
AZO	Aluminum doped zinc oxide
CNA	common neighbor analysis
CNC	centro-symmetry parameter
CNT	carbon nanotube
fcc	face-centered cubic
FF	filling fraction ratio
FFT	fast Fourier transform
ITO	Indium doped tin oxide
KrF	Krypton fluoride
LPW	laser plasmonic welding
MD	molecular dynamic
PDMS	polydimethylsiloxane
PET	polyethylene terephthalate
SEM	scanning electron microscopy
TCE	transparent conductive electrode
TEM	transmission electron microscopy
UV−vis-NIR	ultraviolet−visible-infrared
XRD	X-ray diffraction pattern

estimated from the top-view Fe-SEM images. Transmission electron microscopy (TEM) observation was performed at Titan in Air Force Institute of Technology, in order to characterize the AgNW crystallinity and recrystallization process during welding. Electrical conductance (sheet resistance) was measured by the Jandel Multi Height Probe with RM3000 Test Unit. The bending test and peeling test were carried out by the same probe station, measuring the film sheet resistance before and after bending and peeling. Optical transmittance spectra were measured by lambda 950 ultraviolet−visible and infrared (UV−vis-IR) spectrophotometers. The light scattering was measured by same spectrophotometers with diffusive and specular mode (Figure SF5). X-ray diffraction pattern of AgNW film was characterized by Bruker D8 (Figure SF8).

Fabrication. Ag nanowires are sparsely coated onto 300 nm SiO_2 capped silicon substrate, which has predeposited alignment marks. The randomly distributed cross junctions of two Ag nanowires can be found and located under a 100× optical microscope for further device fabrication process *via* e-beam lithography and e-beam deposition. A 10/50 nm Ni/Au is used as contact metals and gives fairly good contacts. Transport measurements are performed in a Lakeshore Model CPX-VF probe station at room temperature. The single nanowire resistance or cross-junction resistance is measured with a Stanford SR830 lock-in at low-frequency (<20 Hz) excitation current of 1 μA.

Nomenclature, Greek symbols, and abbreviations used in this study are found on Table 1.

Conflict of Interest: The authors declare no competing financial interest.

Acknowledgment. The authors appreciate the financial support from Purdue office of vice president for research (OVPR), Indiana Next Generation Manufacturing Competitiveness Center (IN-MAC) and U.S. Office of Naval Research.

Supporting Information Available: The Supporting Information is available free of charge on the ACS Publications website at DOI: 10.1021/acsnano.5b03601.

Additional experimental details (PDF)
Movie SM1 (AVI)
Movie SM2 (AVI)

REFERENCES AND NOTES

1. Wu, Z.; Chen, Z.; Du, X.; Logan, J. M.; Sippel, J.; Nikolou, M.; Kamaras, K.; Reynolds, J. R.; Tanner, D. B.; Hebard, A. F.; Rinzler, A. G. Transparent, Conductive Carbon Nanotube Films. *Science* **2004**, *305*, 1273–1276.
2. Gordon, R. G. Criteria for Choosing Transparent Conductors. *MRS Bull.* **2000**, *25*, 52–57.
3. Hecht, D. S.; Hu, L.; Irvin, G. Emerging transparent electrodes based on thin films of carbon nanotubes, graphene, and metallic nanostructures. *Adv. Mater.* **2011**, *23*, 1482–513.
4. Gruner, G. Carbon nanotube films for transparent and plastic electronics. *J. Mater. Chem.* **2006**, *16*, 3533.
5. Geng, H.-Z.; Kim, K. K.; So, K. P.; Lee, Y. S.; Chang, Y.; Lee, Y. H. Effect of Acid Treatment on Carbon Nanotube-Based Flexible Transparent Conducting Films. *J. Am. Chem. Soc.* **2007**, *129*, 7758–7759.
6. Gomez De Arco, L.; Zhang, Y.; Schlenker, C. W.; Ryu, K.; Thompson, M. E.; Zhou, C. Continuous, Highly Flexible, and Transparent Graphene Films by Chemical Vapor Deposition for Organic Photovoltaics. *ACS Nano* **2010**, *4*, 2865–2873.
7. Hu, L.; Kim, H. S.; Lee, J.-Y.; Peumans, P.; Cui, Y. Scalable Coating and Properties of Transparent, Flexible, Silver Nanowire Electrodes. *ACS Nano* **2010**, *4*, 2955–2963.
8. Bergin, S. M.; Chen, Y. H.; Rathmell, A. R.; Charbonneau, P.; Li, Z. Y.; Wiley, B. J. The effect of nanowire length and diameter on the properties of transparent, conducting nanowire films. *Nanoscale* **2012**, *4*, 1996–2004.
9. Garnett, E. C.; Cai, W.; Cha, J. J.; Mahmood, F.; Connor, S. T.; Greyson Christoforo, M.; Cui, Y.; McGehee, M. D.; Brongersma, M. L. Self-limited plasmonic welding of silver nanowire junctions. *Nat. Mater.* **2012**, *11*, 241–9.
10. Foygel, M.; Morris, R. D.; Anez, D.; French, S.; Sobolev, V. L. Theoretical and computational studies of carbon nanotube composites and suspensions: Electrical and thermal conductivity. *Phys. Rev. B: Condens. Matter Mater. Phys.* **2005**, *71*, 104201.
11. Han, B.; Pei, K.; Huang, Y.; Zhang, X.; Rong, Q.; Lin, Q.; Guo, Y.; Sun, T.; Guo, C.; Carnahan, D.; Giersig, M.; Wang, Y.; Gao, J.; Ren, Z.; Kempa, K. Uniform self-forming metallic network as a high-performance transparent conductive electrode. *Adv. Mater.* **2014**, *26*, 873–7.
12. Madaria, A.; Kumar, A.; Ishikawa, F.; Zhou, C. Uniform, highly conductive, and patterned transparent films of a percolating silver nanowire network on rigid and flexible substrates using a dry transfer technique. *Nano Res.* **2010**, *3*, 564–573.
13. Zhang, M. Y.; Nian, Q.; Cheng, G. J. Room temperature deposition of alumina-doped zinc oxide on flexible substrates by direct pulsed laser recrystallization. *Appl. Phys. Lett.* **2012**, *100*, 151902–151902−4.
14. Zhang, M. Y.; Nian, Q.; Shin, Y.; Cheng, G. J. Direct pulsed laser crystallization of nanocrystals for absorbent layers in photovoltaics: Multiphysics simulation and experiment. *J. Appl. Phys.* **2013**, *113*, 193506.
15. Spechler, J. A.; Arnold, C. B. Direct-write pulsed laser processed silver nanowire networks for transparent conducting electrodes. *Appl. Phys. A: Mater. Sci. Process.* **2012**, *108*, 25–28.
16. Tang, J.; Tang, D.; Su, B.; Li, Q.; Qiu, B.; Chen, G. Silver nanowire−graphene hybrid nanocomposites as label for sensitive electrochemical immunoassay of alpha-fetoprotein. *Electrochim. Acta* **2011**, *56*, 8168–8175.
17. Zhu, M.; Chen, P.; Liu, M. Graphene Oxide Enwrapped Ag/AgX (X = Br, Cl) Nanocomposite as a Highly Efficient Visible-Light Plasmonic Photocatalyst. *ACS Nano* **2011**, *5*, 4529–4536.
18. Han, S.; Hong, S.; Ham, J.; Yeo, J.; Lee, J.; Kang, B.; Lee, P.; Kwon, J.; Lee, S. S.; Yang, M.-Y.; Ko, S. H. Fast Plasmonic Laser Nanowelding for a Cu-Nanowire Percolation Network for Flexible Transparent Conductors and Stretchable Electronics. *Adv. Mater.* **2014**, *26*, 5808–5814.
19. Schwartz, L. W.; Moussallp, P.; Campbell, P.; Eley, R. R. Numerical Modelling of Liquid Withdrawal from Gravure Cavities in Coating Operations. *Chem. Eng. Res. Des.* **1998**, *76*, 22–28.
20. Harry, G. L. Slot Die Coating for Low Viscosity Fluids. In *Coatings Technology Handbook*, 3rd ed.; CRC Press: Boca Raton, FL, 2005; pp 19−1−19−15.
21. Liu, C. H.; Yu, X. Silver nanowire-based transparent, flexible, and conductive thin film. *Nanoscale Res. Lett.* **2011**, *6*, 75.
22. Chen, H.; Gao, Y.; Zhang, H.; Liu, L.; Yu, H.; Tian, H.; Xie, S.; Li, J. Transmission-Electron-Microscopy Study on Fivefold Twinned Silver Nanorods. *J. Phys. Chem. B* **2004**, *108*, 12038–12043.
23. Wen, X.; Xie, Y.-T.; Mak, W. C.; Cheung, K. Y.; Li, X.-Y.; Renneberg, R.; Yang, S. Dendritic Nanostructures of Silver: Facile Synthesis, Structural Characterizations, and Sensing Applications. *Langmuir* **2006**, *22*, 4836–4842.
24. Ding, C.; Tian, C.; Krupke, R.; Fang, J. Growth of nonbranching Ag nanowires via ion migrational-transport controlled 3D electrodeposition. *CrystEngComm* **2012**, *14*, 875.
25. Lu, Y.; Huang, J. Y.; Wang, C.; Sun, S.; Lou, J. Cold welding of ultrathin gold nanowires. *Nat. Nanotechnol.* **2010**, *5*, 218–24.
26. Nian, Q.; Zhang, M. Y.; Schwartz, B. D.; Cheng, G. J. Ultraviolet laser crystallized ZnO:Al films on sapphire with high Hall mobility for simultaneous enhancement of conductivity and transparency. *Appl. Phys. Lett.* **2014**, *104*, 201907.
27. Li, B.; Wen, X.; Li, R.; Wang, Z.; Clem, P. G.; Fan, H. Stress-induced phase transformation and optical coupling of silver nanoparticle superlattices into mechanically stable nanowires. *Nat. Commun.* **2014**, *5*, 4179.

28. Karim, S.; Toimil-Molares, M. E.; Balogh, A. G.; Ensinger, W.; Cornelius, T. W.; Khan, E. U.; Neumann, R. Morphological evolution of Au nanowires controlled by Rayleigh instability. *Nanotechnology* **2006**, *17*, 5954–5959.
29. Qian, H.; Ma, Y.; Yang, Q.; Chen, B.; Liu, Y.; Guo, X.; Lin, S.; Ruan, J.; Liu, X.; Tong, L.; Wang, Z. L. Electrical Tuning of Surface Plasmon Polariton Propagation in Graphene—Nanowire Hybrid Structure. *ACS Nano* **2014**, *8*, 2584.
30. Song, M.; Chen, G.; Liu, Y.; Wu, E.; wu, B.; Zeng, H. Polarization properties of surface plasmon enhanced photoluminescence from a single Ag nanowire. *Opt. Express* **2012**, *20*, 22290–22297.
31. Baffou, G.; Quidant, R.; Girard, C. Heat generation in plasmonic nanostructures: Influence of morphology. *Appl. Phys. Lett.* **2009**, *94*, 153109.
32. Plimpton, S. Fast Parallel Algorithms for Short-Range Molecular Dynamics. *J. Comput. Phys.* **1995**, *117*, 1–19.
33. Finnis, M. W.; Sinclair, J. E. A simple empirical N-body potential for transition metals. *Philos. Mag. A* **1984**, *50*, 45–55.
34. Williams, P. L.; Mishin, Y.; Hamilton, J. C. An embedded-atom potential for the Cu—Ag system. *Modell. Simul. Mater. Sci. Eng.* **2006**, *14*, 817–833.
35. Stukowski, A. Visualization and analysis of atomistic simulation data with OVITO—the Open Visualization Tool. *Modell. Simul. Mater. Sci. Eng.* **2010**, *18*, 015012.
36. Tsuzuki, H.; Branicio, P. S.; Rino, J. P. Structural characterization of deformed crystals by analysis of common atomic neighborhood. *Comput. Phys. Commun.* **2007**, *177*, 518–523.
37. Lee, S. J.; Kim, Y.-H.; Kim, J. K.; Baik, H.; Park, J. H.; Lee, J.; Nam, J.; Park, J. H.; Lee, T.-W.; Yi, G.-R.; Cho, J. H. A roll-to-roll welding process for planarized silver nanowire electrodes. *Nanoscale* **2014**, *6*, 11828–11834.
38. Kelchner, C.; Plimpton, S.; Hamilton, J. Dislocation nucleation and defect structure during surface indentation. *Phys. Rev. B: Condens. Matter Mater. Phys.* **1998**, *58*, 11085–11088.
39. Langley, D.; Giusti, G.; Mayousse, C.; Celle, C.; Bellet, D.; Simonato, J. P. Flexible transparent conductive materials based on silver nanowire networks: a review. *Nanotechnology* **2013**, *24*, 452001.
40. van de Groep, J.; Spinelli, P.; Polman, A. Transparent Conducting Silver Nanowire Networks. *Nano Lett.* **2012**, *12*, 3138–3144.
41. Stauffer, D.; Aharony, A. *Introduction to Percolation Theory*; Taylor & Francis: Washington, DC, 1992.
42. Lee, J.-Y.; Connor, S. T.; Cui, Y.; Peumans, P. Solution-Processed Metal Nanowire Mesh Transparent Electrodes. *Nano Lett.* **2008**, *8*, 689–692.
43. Kang, M. G.; Guo, L. J. Nanoimprinted Semitransparent Metal Electrodes and Their Application in Organic Light-Emitting Diodes. *Adv. Mater.* **2007**, *19*, 1391–1396.
44. Li, J.; Hu, L.; Wang, L.; Zhou, Y.; Grüner, G.; Marks, T. J. Organic Light-Emitting Diodes Having Carbon Nanotube Anodes. *Nano Lett.* **2006**, *6*, 2472–2477.
45. Chen, R.; Das, S. R.; Jeong, C.; Khan, M. R.; Janes, D. B.; Alam, M. A. Co-Percolating Graphene-Wrapped Silver Nanowire Network for High Performance, Highly Stable, Transparent Conducting Electrodes. *Adv. Funct. Mater.* **2013**, *23*, 5150–5158.
46. Ding, L.; Boccard, M.; Bugnon, G.; Benkhaira, M.; Nicolay, S.; Despeisse, M.; Meillaud, F.; Ballif, C. Highly transparent ZnO bilayers by LP-MOCVD as front electrodes for thin-film micromorph silicon solar cells. *Sol. Energy Mater. Sol. Cells* **2012**, *98*, 331–336.
47. Faraj, M. G.; Ibrahim, K. Optical and Structural Properties of Thermally Evaporated Zinc Oxide Thin Films on Polyethylene Terephthalate Substrates. *Int. J. Polym. Sci.* **2011**, *2011*, 1–4.